1991ApJ...381..137F

THE ASTROPHYSICAL JOURNAL, 381:137–146, 1991 November 1
© 1991. The American Astronomical Society. All rights reserved. Printed in U.S.A.

EVOLUTION OF DUST GRAINS THROUGH A HOT GASEOUS HALO

A. FERRARA,[1] F. FERRINI,[2] J. FRANCO,[3] AND B. BARSELLA[2]
Received 1991 February 19; accepted 1991 April 30

ABSTRACT

The evolution of bare spherical dust grains in the halo of spiral galaxies is analyzed. Two different grain compounds, graphites and astronomical silicates, are considered. The detailed mass and luminosity distributions for the Milky Way and NGC 3198 (considered as representative of the Sb and Sc types, respectively) are used to evaluate the range of possible evolutionary tracks. Aside from radiative and gravitational forces, the effects of drag and sputtering from a gaseous halo are included. A simple isothermal and hydrostatic density structure, with temperatures in the range 3×10^5–10^6 K, has been used for this gaseous halo. Most results depend on the optical properties of dust compounds (or, equivalently, on the radiation pressure coefficients) because the velocities define the final fate of the grains (i.e., destruction in the halo or expulsion from host galaxy). Graphites move faster than silicates, but both types of grains can reach values in excess of 10^2 km s^{-1}. The efficiency for grain destruction increases with (*a*) increasing halo gas temperature, (*b*) decreasing galaxy mass, and (*c*) decreasing radiation pressure coefficients. Thus, silicates behave as a "fragile" grain population in low mass galaxies with a hot ($T \sim 10^6$ K) corona. For a central halo gas density of 0.1 cm^{-3}, spherical silicates with an initial radius of $a = 10^{-5}$ cm lose almost 20% of their mass in time scales between 10^8 and 2×10^8 yr. Some effects of a poloidal magnetic field are also explored along with possible consequences on halo metallicities and intergalactic dust. Grain expulsion can be a common phenomenon in spirals.

Subject headings: galaxies: interstellar matter — interstellar: grains

1. INTRODUCTION

The diffuse cirrus IR emission is smoothly distributed on the whole Galactic disk and seems to be well correlated with the large-scale distribution of gas (Burton 1990). This diffuse emission (along with the new class of "IR-excess clouds," which has a stronger IR emission than the "normal" population of diffuse cirrus clouds; e.g. Désert, Bazell, & Boulanger 1988) extends to high Galactic latitudes and indicates the existence of dust particles even beyond the main gaseous scale height. Other dust tracers also reveal the presence of solid particles outside the gaseous disk. Recent extinction studies with high-latitude A and F stars (Teerikorpi 1990) display a significant amount of polar reddening increasing with z-distance and indicate the presence of dust with a scale height of about 400 pc. Also, a recent analysis of selective extinction and the distribution of refractory elements with distance above midplane (Edgar & Savage 1989) indicates the coexistence of dust and neutral gas up to z-distances of at least 3 kpc (this maximum height is defined by the availability of target stars). The first ionization stage of the refractory elements Ti, Ca, and Fe is present up to these same distances, but their scale heights are well in excess of the one for neutral hydrogen (and, thus, their relative abundance with respect to hydrogen increases with height). A likely origin for the presence of these refractory elements in the gaseous corona, which are heavily depleted inside the disk, is destruction of dust grains at high latitudes.

Evidence for dust outside the main body of external spiral galaxies, as well as in the intergalactic medium, also exists. Sofue (1987, 1990) has reported an impressive evidence of dusty filaments emerging from the disk of the galaxies NGC 253 and NGC 7331. These dusty lanes are rooted into the central 1 or 2 kpc of their host galaxy and extend, curving toward the external parts, for some 2–3 kpc. This particular geometry could be related to the morphology of a magnetic field in the low halo (i.e., charged grains following B-field lines), and may indicate that dusty structures could be used as tracers of the B-field configuration. Additional examples of dusty filaments are found in M82 (Mathis 1973; Telesco, Decher, & Joy 1989), NGC 1808 (Véron-Cetty & Véron 1985; Dahlem et al. 1990), and M81 (M. Peimbert, personal communication). Evidence for intergalactic dust, both in galaxy clusters and also in regions apparently disconnected to any galaxy aggregation has been recently discussed by Rudnicki et al. (1989).

All these studies show that the cool and dusty interstellar phases are either very resistant, so they can withstand the effects of violent expulsion from the disk, or they are gently removed from the main gaseous body. Franco et al. (1991) have discussed a mechanism for a quiet expulsion of the cool gas phases to high Galactic latitudes. Radiation pressure from the stellar disk exerts an upward force on dust grains and this force can push, via dust-gas coupling, diffuse clouds to high Galactic latitudes. This "photolevitation" process, which is similar to the driving agent of cool winds in giant stars (e.g., Salpeter 1974; Kwok 1975), can raise small dusty clouds above the main gaseous disk and generates a "soft" Galactic fountain. Once the dust particles are located above the disk, radiation pressure could also expel bare grains out of the Galaxy (e.g., Chiao & Wickramasinghe 1972; Greenberg et al. 1987; Barsella et al. 1989; Ferrara et al. 1989). Magnetic forces and particle destruction in the hot halo, however, can dominate the bare grain evolution and may prevent such an expulsion. Thus, an important remaining question, which is the one explored here, is the fate of bare dust grains exposed to the halo environment. Different grain compounds have different responses to the ambient conditions and these differences are included in the

[1] Dipartimento di Astronomia, Università di Firenze, Largo E. Fermi 5, 50125 Firenze, Italy.
[2] Dipartimento di Fisica, Università di Pisa, Piazza Torricelli 2, 56100 Pisa, Italy.
[3] Instituto de Astronomía–UNAM, Apdo. Postal 70-264, 04510 México D.F., México.

© American Astronomical Society • Provided by the NASA Astrophysics Data System

1991ApJ...381..137F

analysis. The structure of the paper is as follows. Section 2 outlines the main features of the model, and presents a brief review of the observational evidences related to the gaseous halo conditions. Section 3 describes the forces acting on the grains, and § 4 presents the results for two test galaxies, the Milky Way and NGC 3198, on which the model has been applied. A brief discussion is given in § 5.

2. BASIC MODEL INGREDIENTS

2.1. *Dust Grains*

The basic parameters required to calculate the radiative acceleration of dust particles are their optical properties and internal structure (i.e., size and density for both core and mantle). These, of course, depend on the details of the model chosen for the interstellar grains but, regardless of this specific model, there is a reasonable agreement that dielectric and metallic grains are present in the interstellar space (e.g., Mathis, Rumpl, & Nordsiek 1977; Greenberg & Chlewicki 1983; Williams 1989; Mathis 1990, and references therein). For simplicity, the analysis includes spherical "astronomical silicates" (Draine & Lee 1984) and graphite (e.g., Tosatti & Bassani 1970; Phillip 1977), as representative of dielectric and semimetallic grains, respectively. A variety of other grain components are also present, such as polycyclic aromatic hydrocarbons, but these will not be considered in the present study mainly because they are apparently more fragile and can be easily destroyed by radiation (e.g., Puget & Léger 1989). At the wavelengths of interest here, UV and visible, the optical properties of simple spheres and fractal aggregates (i.e., amorphous grains) of silicates and carbon are very similar (Bazell & Dwek 1990). Thus, the assumed spherical grain geometry does not represent a major restriction.

A radius of $a \sim 0.1$ μm seems to be adequate for a typical interstellar silicate grain (e.g., see Mathis et al. 1977), but graphite grains should have smaller sizes. For simplicity, we choose $a = 0.1$ μm and $\rho = 3.3$ g cm^{-3} as typical parameters for an astronomical silicate, and $a = 0.05$ μm and $\rho = 2.26$ g cm^{-3} for graphite (the corresponding frequency-averaged radiation pressure coefficients, $Q^*_{\rm pr}$, for the average radiation field of Sb and Sc galaxies are shown in Fig. 1, in § 3.1).

2.2. *Mass and Luminosity*

An adequate knowledge of the luminosity and matter distribution of the underneath galaxy is required to compute grain evolution. A spiral galaxy can be properly characterized by three components: bulge, disk, and a dark massive halo. The disk is considered as an infinitely thin axially symmetric exponential distribution of luminosity and matter. The bulge is taken as a massive and luminous addition to the center of the galactic disk, and the halo is considered completely dark with a spherically symmetric mass structure. The relative importance of these components, as well as the properties of the gaseous halo, varies from galaxy to galaxy and a "general" model galaxy is difficult to construct. Thus, one has to work with specific cases and two particular examples, the Milky Way and NGC 3198 (see Appendix), are considered in the models presented in § 3.

2.3. *Gaseous Halo*

The structure of the interstellar medium out of the thin disk, as revealed by the present state of the observational knowledge, is fairly inhomogeneous and complex (see Heiles 1990 and references therein). There is a wide range of physical conditions and a variety of different ionization stages with a complex velocity field (e.g., Danly 1990). The temperature of the observed ions span from $\sim$170 K to about 3×10^5 K (e.g., Savage 1989) but a hotter component (with $T \sim 10^6$ K, or larger) is perhaps also present, as some interpretations of the soft X-ray background observations may suggest (e.g., Marshall & Clarke 1984; see recent review by McCammon & Sanders 1990). The densities are more difficult to evaluate (column densities of heavy element ions provide only information on the corresponding ions; e.g., $\sim 10^{-9}$ cm^{-3} for Ca II), but the gas seems to be stratified with a variety of different scale heights (e.g., Edgar & Savage 1989). Actually, the H I gas displays two different vertical stratifications: a thin Gaussian structure (the "main" disk) and an extended exponential tail (e.g., Dickey & Lockman 1990). The neutral gas density outside the main gaseous disk seems to be below $\sim$0.1 cm^{-3} (e.g., Dickey & Lockman 1990), whereas the density of free electrons has values below $\sim$0.01 cm^{-3} (e.g., Reynolds 1989).

This complex mixture of different gas phases, which certainly challenge the "common conceptions" (e.g., Cox 1990; see also Scalo 1990), is difficult to include in a simple global model and a single-temperature gaseous halo is considered here. The adopted temperatures are in the range 3×10^5–10^6 K, and the observed low-temperature components are neglected. The gas is in hydrostatic equilibrium with the global galactic gravitational field and corotates with the disk. This assumption, as pointed out by Savage (1989), should be valid at least for the lower parts of the halo. The assumed gas temperatures may provide a reasonable description of the sputtering process, but the absence of the cooler and denser components may lead to a slight overestimation of the grain velocities. Hence, as pointed out by the referee, the calculations of this paper mostly relate to the region with $z > 1$ kpc. The density at the halo base is assumed to decrease exponentially with galactocentric radius, and has the same scale length of the surface disk density (see Fig. 2 in § 3.2).

2.4. *Magnetic Fields*

The strength and morphology of B-fields in the disk of the Milky Way, and in the disk of some external spiral galaxies, has been derived with a certain detail (e.g., Sofue, Fujimoto, & Wielebinski 1986; Ruzmaikin 1987; Rand & Kulkarni 1989; Beck 1990). The general average field directions are parallel to the spiral disks, with average strengths between 2 and 10 μG but display random fluctuations at almost any scale. In contrast with the rest of the disk, the central regions of our Galaxy and the cores of active galaxies have a poloidal field configuration (i.e., the field direction runs perpendicular to the Galactic plane; e.g., Seiradakis et al. 1985; Reich 1988; Lesch et al., 1989).

The halo field of our Galaxy, on the other hand, has been inferred with statistical studies of Faraday rotation of extragalactic sources and the best estimates for the field above $z \sim 500$ pc indicate strengths of the order ~ 1 μG (e.g., Sofue et al. 1986), not much different from the average disk value, ~ 3 μG. Magnetic fields have also been detected in the halo of external galaxies through radio continuum observations (Hummel, van Gorkom, Kotanyi 1983; Sofue et al. 1986; Beck 1990). Data interpretation is often very difficult and only few details are known about these so-called radio-halos. The field strengths, usually derived from equipartition, are also of the order of μG whereas the halo field "thickness," or scale height,

© American Astronomical Society • Provided by the NASA Astrophysics Data System

1991ApJ...381..137F

varies from 1 to 8 kpc (an impressive case with a strong poloidal halo field is the edge-on galaxy NGC 4631, which shows a B_z component with a scale height of about 8 kpc; e.g., Hummel, Beck, & Dahlem 1991). These values are small compared to the expected halo dimensions and may be indicative of a weak global halo field. The connection of these fields with the intergalactic medium, if any, is even less known. The measured average global fields in some galaxy clusters are also on the range of μG, but the intergalactic medium has a very weak (or absent) field with upper limits in the range 10^{-10} to 10^{-11} μG (see Vallée 1990).

From the theoretical point of view it is likely that, superposed on the large-scale field structure of galaxies, there exists a fluctuating component localized in the lower regions of the halo ($z \leq 1$ kpc). Here, due to Parker instabilities in the disk or to a strong star-forming activity, an increasing amount of magnetic lines normal to the plane can be generated (e.g., Parker 1966; Sofue et al. 1986; Hummel et al. 1991; Matsumoto & Shibata 1990). Following the prescriptions of the $\alpha\omega$-dynamo theory (e.g., Ruzmaikin 1987), the ratio of the halo and disk fields is inversely proportional to the square root of the maximum rotation velocity of the galaxy. For the Milky Way, having a peak rotation velocity of about ~ 230 km s^{-1}, the dynamo model predicts that the global halo B-field should be much smaller than the one in the disk (similar arguments can be brought for NGC 3198, which rotates at about ~ 220 km s^{-1}). This result could be consistent with the values inferred from Faraday rotation studies for the halo of our Galaxy if the field decays rapidly within a few kpc (i.e., if the observational results are weighted toward the disk-halo interface). This is a very likely possibility, also consistent with the very small upper limits inferred for the intergalactic field, but there is no consensus on the appropriate value for the intensity of global halo field (e.g., Sofue et al. 1986).

Given such a complex and uncertain situation, two simple test cases were considered: (1) a model without magnetic field, corresponding to the case of a quiet radio halo and "free" grain evolution, and (2) a model with a constant 1 μG B-field in the z-direction, corresponding to a poloidal field case with strong radio emission. This magnetic configuration (which favors cosmic-ray support of the gaseous halo; e.g., Hartquist & Morfill 1986) seems to represent a good approximation, at least in the lowest halo regions, where dust is expected to move. A dipole field is not considered here because, even when not ruled out by observations, the available evidences do not indicate such a morphology. A case with random fluctuations is certainly relevant but, unfortunately, is beyond the present possibilities of our model.

3. THE GLOBAL FORCE FIELD

This section outlines the forces acting on a single dust grain, extending the force field description presented by Barsella et al. (1989) to include magnetic and drag forces. For the sake of simplicity, the notation of Barsella et al. is adopted in this paper, and the reader is referred to their work for a detailed description of the force vectors on the chosen axisymmetric coordinates.

3.1. *Radiative and Gravitational Forces*

The gravitational force on a grain of mass m_g can be written as

$$\boldsymbol{F}_G(\boldsymbol{r}) = m_g \boldsymbol{G}(\boldsymbol{r}) , \tag{1}$$

where $\boldsymbol{G}(\boldsymbol{r})$ is the gravitational field produced by the galactic mass distribution (bulge, disk, and dark massive halo) at the grain position $\boldsymbol{r}$. The expression for the radiation pressure force is formally more complicated

$$\boldsymbol{F}_R(\boldsymbol{r}) = \pi a^2 \int d\boldsymbol{\rho} \int d\nu Q_{\rm pr}(a, \nu) \boldsymbol{\Psi}(\boldsymbol{r}, \boldsymbol{\rho}, \nu) , \tag{2}$$

where $Q_{\rm pr}(a, \nu)$ is the radiation pressure coefficient for a spherical grain of radius a at the frequency ν, $\boldsymbol{\Psi}(\boldsymbol{r}, \boldsymbol{\rho}, \nu)$ is the radiation field at frequency ν generated by a galactic element located at $\boldsymbol{\rho}$ and reaching the grain position, $\boldsymbol{r}$ [i.e., $\boldsymbol{\rho}$ is the radial vector position on the plane of the disk, $R = |\boldsymbol{\rho}|$ is the galactocentric distance on the plane of the disk, and $r = |\boldsymbol{r}| = (R^2 + z^2)^{1/2}$ is any radial distance from the center of the galaxy]. The radiation force is assumed to be continuous at any point in space, and two additional simplifying suppositions are included: the spectral form of the disk emission is assumed independent of the galactocentric location, $\boldsymbol{\rho}$, and the bulge is considered as a point source in the center of the disk.

With these simplifications, the radiation field function can be written as

$$\boldsymbol{\Psi}(\boldsymbol{r}, \boldsymbol{\rho}, \nu) = \boldsymbol{\Xi}(\boldsymbol{r}, \boldsymbol{\rho}) \Omega(\nu) , \tag{3}$$

where $\Omega(\nu)$ is the normalized spectral function [i.e. $\int \Omega(\nu) d\nu = 1$], and $\boldsymbol{\Xi}(\boldsymbol{r}, \boldsymbol{\rho})$ contains the total flux from each galactic disk element $\boldsymbol{\rho}$ diluted by the geometric factor $1/4\pi(\boldsymbol{r} - \boldsymbol{\rho})^2$. Integration of $Q_{\rm pr}(a, \nu)$ over the spectral function gives the frequency averaged $Q^*_{\rm pr}$, which is now only a function of the grain radius, and the expression for the radiative force becomes

$$Q^*_{\rm pr}(a) = \int d\nu Q_{\rm pr}(a, \nu) \Omega(\nu) , \tag{4a}$$

$$\boldsymbol{F}_R(\boldsymbol{r}) = \pi a^2 Q^*_{\rm pr}(a) \int d\boldsymbol{\rho} \boldsymbol{\Xi}(\boldsymbol{r}, \boldsymbol{\rho}) = \pi a^2 Q^*_{\rm pr}(a) \boldsymbol{\Gamma}(\boldsymbol{r}) . \tag{4b}$$

Following Pence (1976) and Yoshii & Takahara (1988), which give the spectrum between 1400 and 8000 Å for various types of galaxies, we have considered the specific spectral function $\Omega(\nu)$ for each Hubble type. This represents a substantial improvement with respect to the blackbody spectrum assumed by Barsella et al. (1989), and the frequency-averaged radiation pressure coefficients, $Q^*_{\rm pr}$, over the radiation fields of Sb and Sc galaxies are displayed in Figure 1. The figure shows the variations of $Q^*_{\rm pr}$ for silicate and graphite spheres with different radii. In general, graphite grains have higher values of $Q^*_{\rm pr}$ and, thus, have a stronger response to radiation forces than silicates. Similarly, Sc galaxies are a bit more efficient than Sb galaxies at small grain radii but the relation is inverted at larger grain radii.

3.2. *Gas Drag in the Halo*

The halo gas is assumed isothermal, with temperatures in the range 3–10 × 10^5 K, and in hydrostatic equilibrium. Figure 2 shows a typical density distribution for the hot halo gas in the Milky Way.

The interactions (drag and sputtering) with this hot halo material play a crucial role in the evolution of grains, as it has been stressed for the gas in the disk by Draine & Salpeter (1979). They give a comprehensive description of the interactions with ionized gas, and we use their results to evaluate these interactions with a pure hydrogen plasma. The total drag

© American Astronomical Society • Provided by the NASA Astrophysics Data System

1991ApJ...381..137F

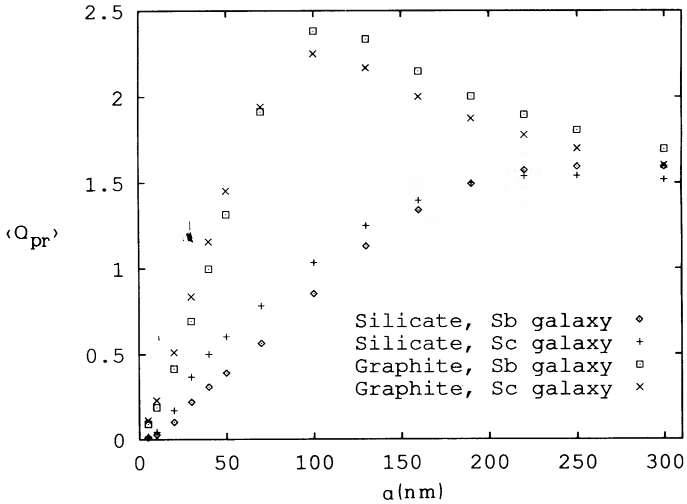

FIG. 1.—Frequency-averaged radiation pressure coefficients, $Q^*_{\rm pr}$, for Sb and Sc galaxies (silicate and graphite grains) vs. grain radius.

force acting on a charged grain is

$$F_{\rm drag} = 2\pi a^2 nkT[G_0(s) + Z^2\phi^2 \ln(\Lambda/Z)G_2(s)] , \quad (5)$$

$$G_0(s) = \left(s^2 + 1 - \frac{1}{4s^2}\right) {\rm erf}\,(s) + \left(s + \frac{1}{2s}\right)\frac{e^{-s^2}}{\sqrt{\pi}} , \quad (6)$$

$$G_2(s) = \frac{{\rm erf}\,(s)}{s^2} - 2\,\frac{e^{-s^2}}{s\sqrt{\pi}} , \quad (7)$$

$$\phi = \frac{eU}{kT} , \quad (8)$$

$$s = \left(\frac{m_{\rm H} v^2}{2kT}\right)^{1/2} , \quad (9)$$

$$\Lambda = \frac{3}{2ae\phi}\left(\frac{kT}{\pi n_e}\right)^{1/2} , \quad (10)$$

where v is the grain speed, T is the gas temperature, n is the ion number density, n_e is the electron number density, $m_{\rm H}$ is the proton mass, a is the grain radius, e is the unit charge, $Z = 1$ is the ion charge number, and U is the electrostatic potential of the grain. The function G_0 contains the terms of the collisional drag, and G_2 is associated to the Coulomb drag. The grain potential and the evolution of the grain radius are described below.

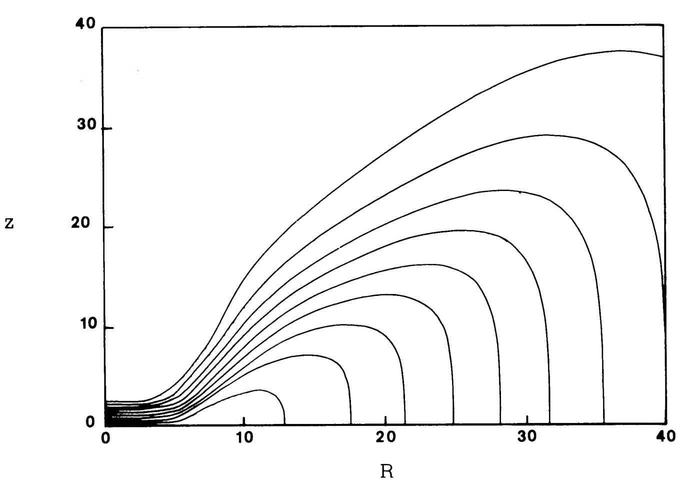

FIG. 2.—Density contours for the hot halo model. The particle density of the top curve is 0.01 cm^{-3}; the contours are separated by 0.01, increasing downside.

3.2.1 *Charge of Grains*

Different mechanisms may contribute to the grain charge: electron and ion sticking, secondary electron emission, photoelectric effect, and field emission of electrons. The gas volume density in the halo is substantially smaller than the one in the disk, and the ambient starlight has a strong contribution to the grain charging, which is always positive under these circumstances (this case is referred to as Model B by Draine & Salpeter 1979). For gas temperatures in the interval 0.3–1 $\times$ 10^6 K, the steady state values of the grain potentials (see Table 2 and Figs. 1 and 2 of Draine & Salpeter) are $U \sim 5$ V for silicates with $a = 0.1$ μm, and $U \sim 3$ V for graphite grains with $a = 0.01$ μm.

For simplicity, these values have been adopted, and, given that random variations of the grain charge are likely to occur, some small fluctuations around the mean steady state charges have also been allowed for. This was done by simulating a random variation of the grain charge at each time step; the charge is randomly increased or decreased during each integration, limiting the total amplitude of the fluctuation to a few percent. The total charge accumulated onto the grain surface by these fluctuations is always less than the one necessary to disrupt the grains (the critical potential for disruption of the grains considered here is of the order of $U \simeq 10^3$ V, much higher than the values ever reached with the random fluctuations).

3.2.2. *Sputtering*

Direct grain-ion collisions at high ion temperatures, or large grain speeds, can erode the grain (cosmic rays may also have an erosion effect, but this process is less efficient; e.g., Barlow 1978; Draine & Salpeter 1979). The continuous reduction of grain dimensions, which changes its response to radiative forces (see Fig. 1), can eventually disintegrate the particle. The final outcome of grain evolution through the gaseous halo, then, is very sensitive to sputtering: ejection from the host galaxy, even when allowed by the global radiative field, is in some cases totally inhibited by particle destruction. Besides, the release of atoms constituting the external dust layers pollutes with heavy elements the regions crossed by the grains, modifying the local chemical abundances (this point is further discussed in § 4.2).

The sputtering rate for spherical grains interacting with protons is (Draine & Salpeter 1979)

$$\frac{dN}{dt} = a^2\left(\frac{2\pi kT}{m}\right)^{1/2} n\,\frac{e^{-s^2}}{s}\int_{\epsilon_{\rm min}}^{\infty} d\epsilon\,\epsilon^{1/2}$$
$$\times\left(1 - \frac{Z\phi}{\epsilon}\right)e^{-\epsilon}\,\sinh\,(2\epsilon^{1/2}s)\langle Y(E)\rangle_\theta , \quad (11)$$

where $\epsilon_{\rm min} = \max\,[0, Z\phi]$, and $\langle Y(E)\rangle_\theta$ is the sputtering yield (target molecules per projectile) for projectiles of kinetic energy $E = (\epsilon - Z\phi)kT$, averaged over the incidence angle θ with respect to the surface normal. Given the range of halo gas temperatures considered here, the low-energy sputtering yield discussed by Draine & Salpeter was used.

© American Astronomical Society • Provided by the NASA Astrophysics Data System

1991ApJ...381..137F

3.3. *Lorentz Force*

A charged grain moving with a velocity $\boldsymbol{v} = d\boldsymbol{r}/dt$ in a magnetic field $\boldsymbol{B}$ feels a force $\boldsymbol{F}_L = qe(\boldsymbol{v} \times \boldsymbol{B})/c$, where qe is the grain charge. For the typical values of the quantities involved (i.e. a ~ 0.1 μm grain with $U \sim 3$–5 V, and $B = 1$ μG), the Larmor radius is very small compared to the scale length of the motion along the field lines (see Shull 1977). The main dynamical effect of the inclusion of the magnetic field, then, is to constrain the motion of the dust particle, and the field lines simply act as tracks for the grain motion. Hence, charged dust grains can be good tracers of the magnetic field configuration in the halo. Observational indications of this possibility in external galaxies have been already emphasized by Chiao & Wickramasinghe (1972) and Sofue (1987, 1990).

These small Larmor radius values, on the other hand, impose a severe computational constraint in modeling magnetic cases: there is no numerical scheme available that can calculate, with the required resolution, the details of the evolution over the range of physical dimensions imposed by the problem. Thus, magnetic cases are explored only within initial galactocentric radius smaller than 1 kpc.

4. EVOLUTION OF GRAINS

4.1. *Test Galaxies*

The light distribution of many spiral galaxies is well established, whereas the mass distribution is usually poorly known (particularly in the massive halo component). Two galaxies have been selected as test cases for our model: the spiral NGC 3198 (e.g., Burstein & Rubin 1985; Ferrara et al. 1990), whose dynamical properties and surface photometry are well known, and the Milky Way. They can be considered as representative of the Sc and Sb types, respectively, and their properties are summarized in the Appendix. Barsella et al. (1989) applied their static force analysis to NGC 3198 and have presented the total force vector fields for silicates and graphites (and for a variety of different grain radii). Their figures, then, represent a very useful complement to the present results.

4.2. *Model Results*

The dynamical evolution of silicate and graphite grains, under the action of the forces discussed in § 3, was obtained by numerical integration of the equation of motion in cylindrical coordinates. Many different models were made, covering a large region of the parameter space, and the results of some selected models are presented here. The adopted initial grain radii were $a = 0.1$ μm, for silicates, and 0.05 μm, for graphite. The initial positions were chosen at a fixed distance above the galactic midplane, $z_0 = 200$ pc, and at a variety of galactocentric distances, R_0, ranging from 0.1 to 8.0 kpc. The grains had zero initial velocity relative to the gas, and two cases for the isothermal gaseous halo are presented. Both halo models have the same base density at the galactic center ($n = 0.1$ cm^{-3}), but, to explore the effects of gas temperature, they were set to different temperatures: $T = 3 \times 10^5$ K and $T = 10^6$ K (these cases will be referred to as the "warm" and "hot" halo, respectively).

Although the two test galaxies belong to different Hubble types and have different mass and luminosity distributions (the Milky Way is of an earlier Hubble type and is more massive and luminous), the general qualitative features of grain circulation have a similar behavior in both cases. One difference is that the grain velocities achieve larger values and hence reach outer positions in shorter time scales, in the case of the Milky Way. This is due to the stronger radiation field, and hence larger radiative force, of our Galaxy (see Appendix). Another difference is associated to the dimensions of the gaseous halo. For any given temperature, the scale height of the gaseous halo increases with decreasing galaxy mass. Thus, smaller galaxies (NGC 3198 in the present study) have more extended gas envelopes and are more efficient in destroying dust grains. This effect is more pronounced in grain compounds with smaller radiation pressure coefficients because their evolutionary time scales are longer, and silicates are more easily destroyed than graphites.

4.2.1. *Dynamical Properties*

Figures 3*a* and 3*b* show the velocity components for a silicate grain evolving through a hot gaseous halo without magnetic field. Velocities are measured from an inertial reference frame (i.e., nonrotating) with origin at the galaxy center: $v_p = (v_{\rm rot}^2 + v_r^2)^{1/2}$ represents the velocity parallel to the galactic plane (where $v_{\rm rot}$ is the rotational velocity and v_r is the radial component), and v_z is the component perpendicular to the plane. The z-component of the angular momentum vector, L_z, is conserved during grain evolution and $v_{\rm rot}$ decreases as the dust particle moves outward. The conservation rule for L_z is strictly valid in the nonmagnetic cases but, given the small Larmor radius, it also holds approximately in the magnetic ones. The velocities are plotted as a function of time, and the initial galactocentric radius is $R_0 = 2$ kpc. Figure 3*a* corresponds to the Milky Way and Figure 3*b* to NGC 3198. The resulting evolutionary tracks in z and R are shown in Figures 3*c* and 3*d*.

The z-velocity component in the Milky Way reaches a peak value, after some 25 Myr, of about 700 km s^{-1}, and decreases afterward. A similar trend appears in the case of NGC 3198, but the peak velocity value is smaller (i.e., $v_z \sim 280$ km s^{-1} at about 30 Myr). Also, the silicate grains are expelled from both galaxies, but the final grain size is smaller for NGC 3198. The details of the grain radius evolution are discussed in the next subsection.

Figure 4 shows another silicate model in the Milky Way with the same initial conditions as the previous one, but with the warm gaseous halo. The velocity decrease is smoother in this case. Given that the isothermal scale height increases with gas temperature, the average gas density in the warm halo case is lower and hence the final velocity is higher. Similarly, given the larger velocity values, the overall sputtering effect is less effective. As a result, compared to the hot halo case, the silicate grain is expelled out of the Galaxy with a larger fraction of its initial mass.

When a grain starts its evolution from a more external galactocentric radius, the z-velocity components are reduced because the radiation field (and, hence, the upward force) becomes weaker with increasing R. Figure 5 shows the evolution, starting from $R_0 = 8$ kpc (i.e., the solar circle), for a silicate grain in the Milky Way with the hot halo. Some features are, roughly speaking, similar to those displayed in Figure 3*a* (i.e., the velocities reach a maximum and then decrease), but now the maximum z-velocity is lowered by a factor of ~ 4.7 and the maximum value of v_p decreases to 230 km s^{-1}.

Graphite grains have a stronger response to radiative forces (see Fig. 1) and, given any initial location, their resulting velocities are larger than the ones for silicates. This is illustrated in Figure 6 for a graphite grain with $a = 0.05$ μm evolving in the

© American Astronomical Society • Provided by the NASA Astrophysics Data System

1991ApJ...381..137F

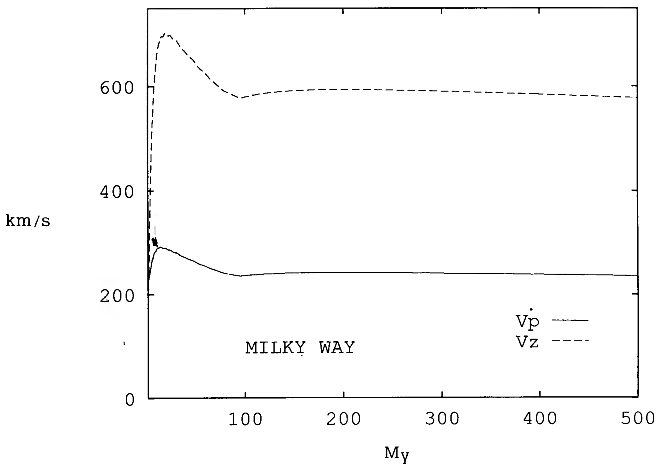

FIG. 3*a*

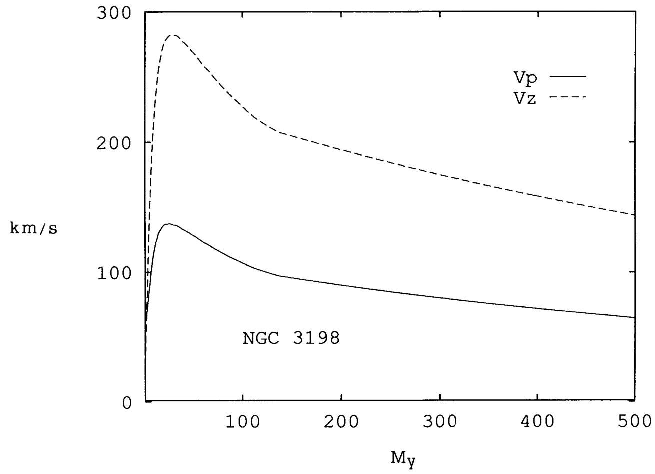

FIG. 3*b*

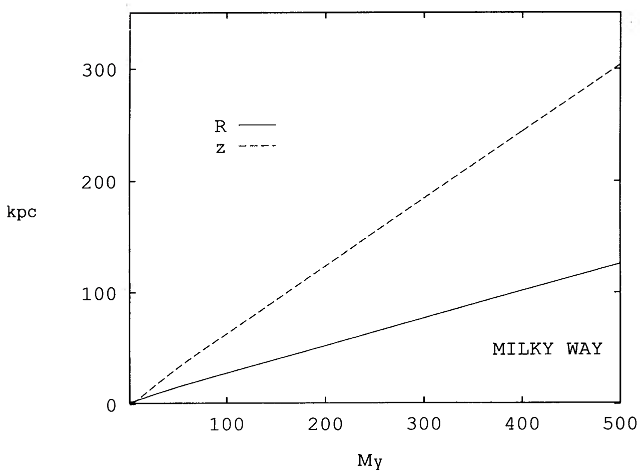

FIG. 3*c*

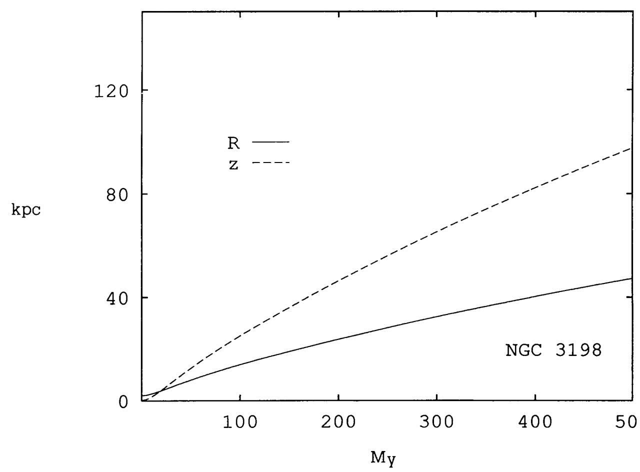

FIG. 3*d*

FIG. 3.—Velocity components, v_p and v_z, for a silicate grain (no magnetic field) plotted vs. time in millions of years; the initial galactocentric distance is $R_0 = 2.0$ kpc. Fig. 3*a* corresponds to the Milky Way and Fig. 3*b* to NGC 3198. The resulting *z* and *R* displacements vs. time are shown in Figs. 3*c* and 3*d*, respectively.

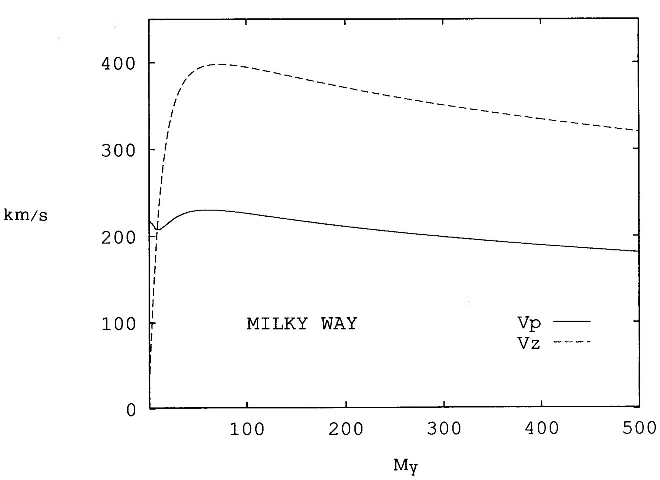

FIG. 4.—As Fig. 3*a*, for a warm gaseous halo

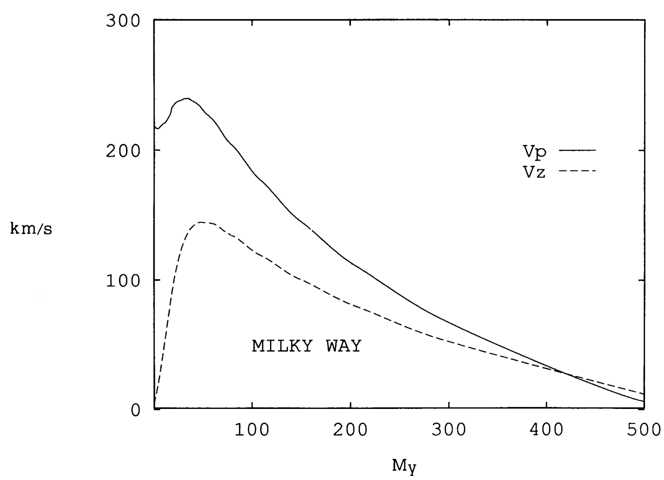

FIG. 5.—As Fig. 3*a*, with $R_0 = 8.0$ kpc

© American Astronomical Society • Provided by the NASA Astrophysics Data System

1991ApJ...381..137F

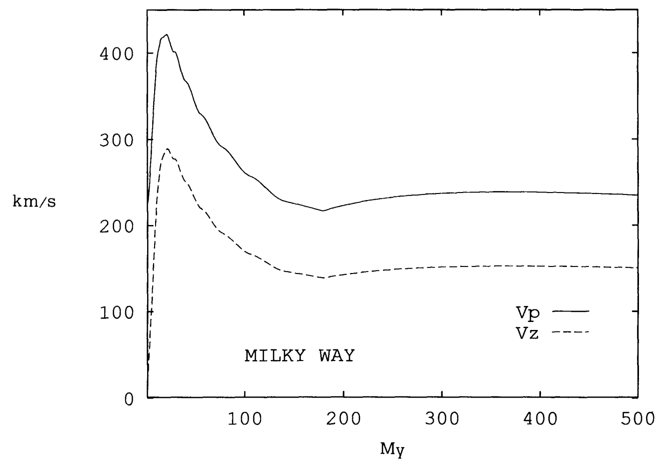

FIG. 6.—As Fig. 5, for graphite grains

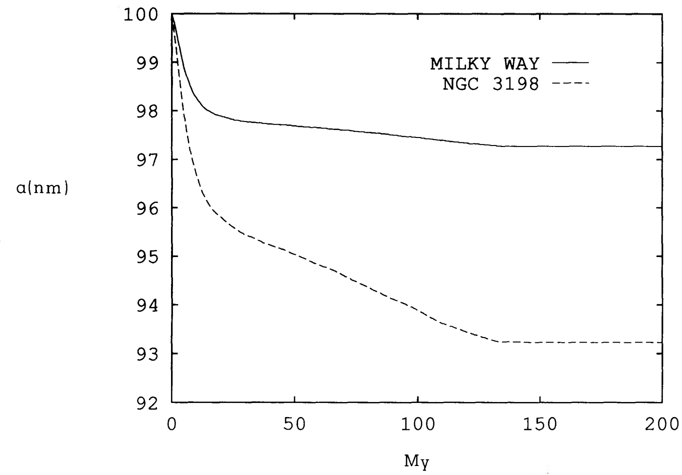

FIG. 8.—Grain radius evolution vs. time for silicate grains in the Milky Way and NGC 3198 ($R_0 = 2.0$ kpc and hot halo case).

Milky Way with a hot halo. The initial galactocentric radius is $R_0 = 8$ kpc. The peak velocities are $v_z \sim 290$ km s^{-1} and $v_p \sim 420$ km s^{-1}.

A brief summary of the dynamical evolution, without *B*-fields, for silicates and graphites in the hot halo of the Milky Way is given in Figures 7*a* and 7*b*. The figures show *z* versus *R* tracks for initial R_0 values of 1, 3, 5, 7, and 9 kpc; the evolution has been followed for 500 Myr. Grains starting from more external galactocentric radii reach lower *z*-heights, as expected from the decreasing radiation field. The response of silicates and graphites to the global force field, on the other hand, is rather different and the dynamical time scales for expulsion are shorter for graphites.

The effect of a poloidal magnetic field is straightforward: a charged grain follows the field lines and evolves on constant $R = R_0$ tracks. Thus, cases with a poloidal magnetic field are not very interesting from the dynamical point of view. They do, however, show a different grain radius evolution, and an example of the magnetic evolution is discussed below.

4.2.2. *Heavy Element Release*

An interesting process taking place during the permanence of grains in the hot gas of the halo is the release of heavy atoms. Sputtering effects depend, as already mentioned, on the ambient gas temperature, grain velocity, and charge. The amount of heavy elements released, and its corresponding grain size reduction, is governed by the time scale for grain destruction (at the plasma density and temperature) and the time required to reach the outskirts of the gaseous halo. For a given halo gas density, larger temperatures have shorter destruction times and, also, result in larger isothermal scale heights. These two properties cause a steep increase in the probability of grain destruction with temperature. Larger grain velocities, on the other hand, have associated shorter halo crossing times and result in a smaller overall sputtering effect. Thus, the net result is that the destruction rate (and, hence, the possibility of grain ejection) is governed by the halo gas properties and the optical grain properties.

Figure 8 shows the evolution of the grain radius, *a*(*t*), for the two silicate models presented in Figure 3 (i.e., $R_0 = 2$ kpc and the hot halo, for both the Milky Way and NGC 3198). The grain radius decreases monotonically as the particle evolves through the dense halo parts and remains constant after the grain reaches the outskirts of the halo. For the Milky Way

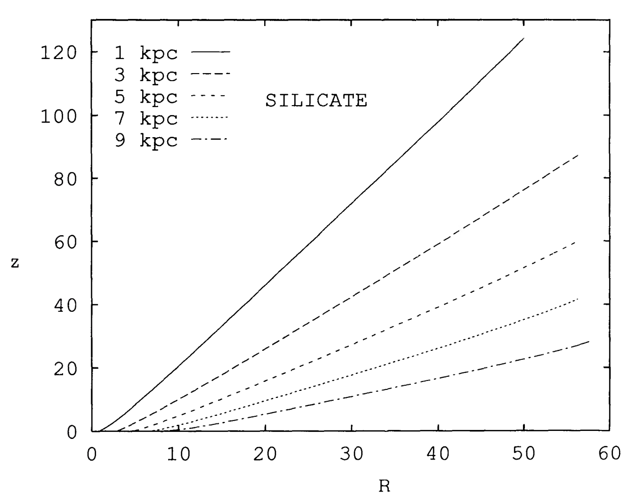

FIG. 7*a*

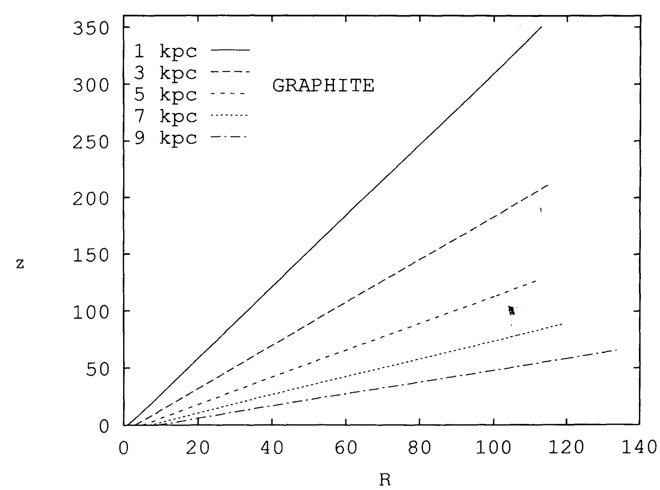

FIG. 7*b*

FIG. 7.—Grain trajectories for the hot halo model of the Milky Way: (*a*) Silicate grains and (*b*) graphite grains. The various curves correspond to different initial galactocentric distances. The height on the disk (*z*) and the radial distance in the Galactic plane (*R*) are in kpc.

© American Astronomical Society • Provided by the NASA Astrophysics Data System

1991ApJ...381..137F

case, it loses about 10% of its mass in a time scale of $\sim 2 \times 10^8$ yr and moves a distance of about 120 kpc. The same case for NGC 3198 shows an enhanced sputtering of the grains which is mainly due to the lower grain velocities for this galaxy. The mass lost by silicates is about 20% of the initial one in 150 kpc.

The main difference between silicates and graphites is that graphites are less affected by sputtering. This is a direct consequence of their shorter transit times through the densest parts of the halo. Graphite grains could then be expelled from their host galaxy, maintaining a higher fraction of their initial mass.

In the warm halo case (presented in Fig. 5), the silicate grain loses only 20% of its mass before reaching the outskirts of the gaseous halo; therefore grain expulsion is more likely. In either halo case, however, a good fraction of the grain mass pollutes the surrounding gas.

Figure 9 shows a magnetic model for a silicate in NGC 3198 with the hot halo. The initial location is $R_0 = 0.2$ kpc, and the poloidal field strength is 1 μG. The main difference with the corresponding nonmagnetic model at the same R_0 is that the helical motion increases the path length required to reach the same height. The z-velocity components are similar in both cases and the grain reaches the same z-distances in about the same time, but it interacts with a larger gas column density in the magnetic case. For sputtering effects, this means a higher efficiency, and the grain radius decreases more quickly.

5. CONCLUSIONS

Radiation pressure from starlight represents an efficient engine to circulate dust particles through the halo of spiral galaxies and, under certain circumstances, can even expel dust into the intergalactic medium. The effects of this pressure are obviously more pronounced in the vicinity of strong radiation fields (see Franco et al. 1991): given the exponential decrease in surface luminosity, the inner regions of spirals are certainly more "active" than the external parts. Similarly, the grain optical properties are key parameters in defining the final state of the circulating particles: graphite has a stronger response to radiative forces and reaches higher velocities than silicates. For typical parameters of Sb and Sc galaxies, both types of grains are accelerated to velocities of the order of hundreds of kilometers per second and are substantially sputtered through

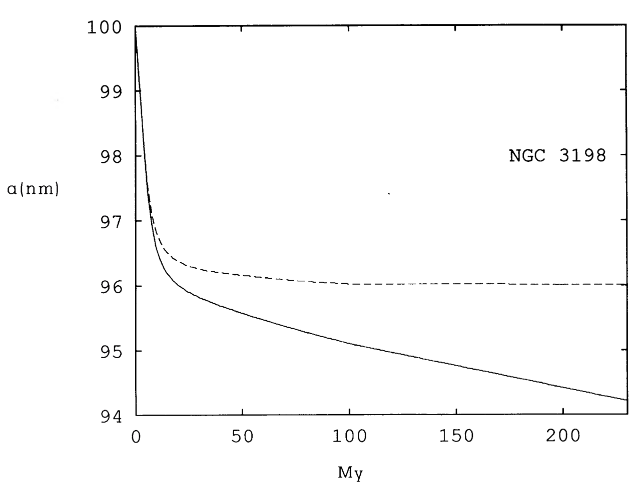

FIG. 9.—Grain radius evolution vs. time for a silicate grain with magnetic field (*solid line*) and without (*dashed line*) for NGC 3198. $R_0 = 0.2$ kpc, hot halo.

their evolution in the halo. The final amount of sputtered mass and, hence, the possibility of expulsion from the host galaxy depends on grain composition and halo conditions.

For a pure hydrogen plasma at the temperatures considered here, the resulting sputtering yields (low-energy yields; Draine & Salpeter 1979) for silicates and graphite are very similar but the total amount of grain mass eroded by the plasma depends on grain composition in two different ways. First, for any given gaseous halo density and temperature, the sputtering rate decreases with grain velocity as e^{-v}/v and graphites, which are the "fast" grains, lose less mass per unit time than silicates. Second, the halo crossing time also decreases with velocity. Fast particles reach the outskirts of the halo in shorter time scales and the total grain mass sputtered by the hot plasma is substantially reduced at high grain speeds. Thus, graphite not only has a smaller sputtering rate but the sputtering process is operating for a shorter period of time. As a result, graphite grains retain a good fraction of their mass and can be expelled from the host galaxy, whereas silicate grains behave as a "fragile" population of dust particles which can be easily destroyed during halo evolution. Given that grain velocities are sensitive functions of the optical properties, the obvious conclusion is that the total amount of sputtered mass and the possibility of expulsion are functions of the optical properties.

There exist a variety of mass models for our Galaxy (e.g., Bahcall, Schmidt & Soneira 1983; Allen & Martos 1986; van der Kruit 1987), and some details of the grain evolution depend, of course, on the details of the model adopted for the mass distributions. The differences among these models, however, are basically associated with differences in parameterization rather than with physical differences. A number of test runs with a variety of different mass distributions were performed (in particular, the mass of the dark halo was varied over one decade), but the peak grain velocities did not vary more than 20%. The main variations appeared in the extension of the gaseous halo (i.e., differences in the gravitational field strength result in differences in the gaseous halo scale height), and hence the sputtering rate did show substantial modifications. Thus, the details of the grain radius evolution are very model-dependent but the dynamical features here described are almost independent of the choice in mass model.

The chemical enrichment of the halo, on the other hand, proceeds in a completely different way from that of the intergalactic medium. The halo is mainly polluted by gas phase refractory elements eroded from the surface of circulating grains, whereas the intergalactic medium should be preferentially polluted by the solid leftovers of this erosion process. Thus, intergalactic dust should be mainly composed by small-sized grains, small compared to the disk component. Also, collisions with the energetic ions can cause deep modifications in the crystalline structure of some types of grains. For instance, in the case of graphite they may lead to the formation of amorphous carbon grains (i.e., Williams 1989). The final fate of this dust population, on the other hand, will depend on the particular conditions prevailing in the surroundings of the ejecting galaxy. In particular, galaxy clusters with X-ray emission have a hot intercluster plasma which will eventually destroy the expelled dust, but grains can survive for very long periods of time in less agressive environments. These aspects are relevant to the discussions on dust obscuration of QSOs (see Ostriker, Vogeley, & York 1990) and may have deeper consequences in the epoch of galaxy formation. Given the expected high star formation rates and the softer potential well,

© American Astronomical Society • Provided by the NASA Astrophysics Data System

1991ApJ...381..137F

any dust formed during those early stages was subjected to strong radiative forces and grain circulation could have been performed at even larger speeds. Dust expulsion, then, could have contaminated pristine regions and could have triggered the formation of further protogalaxies.

Evidences for intergalactic dust are rapidly accumulating (e.g., Hoffmeister 1962; Okroy 1965; Rudnicki et al. 1989 and references therein) and may indicate that dust expulsion is a common phenomenon. In a closely related type of study, Devereux & Young (1990) analyzed the gas-to-dust mass ratio in 58 spirals using the *IRAS* data. They found a mean ratio of ~ 1080, which is a factor of about 10 higher than the one measured in the solar neighborhood. Given that the mass ratio seems to scale almost inversely with heavy element abundances (e.g., Bouchet et al. 1985; Franco & Cox 1986) and there is no indication that these spirals are chemically poor, Devereux & Young concluded that 80%–90% of the dust should be locked in a cold component with a temperature lower than 15 K (radiating at $\lambda > 100$ μm). However, the far-infrared continuum emission of spirals (Eales, Wynn-Williams, & Duncan 1990) can be explained by a single temperature ($T \sim 30$–50 K) dust, and there is no evidence for the proposed cold dust component. The problem of the high gas-to-dust mass ratio is certainly open, but radiation pressure may held responsibility in removing dust from the disk and increasing the mass ratio. This consideration is strengthened by the very high (~ 2100) ratio observed in M82, which is a starburst galaxy where a great amount of dust has been observed in the halo.

We acknowledge the useful comments provided an anonymous referee. J. F. acknowledges a travel grant from CONACyT-Mèxico.

APPENDIX

1. THE SPIRAL GALAXY NGC 3198

There is no evidence for a bulge in this galaxy (Wevers 1984), and the expression for the adopted disk luminosity profile is

$$I(R) = I_0 e^{-\lambda_d R} , \tag{A1}$$

where $I_0 = 119.3\ L_\odot\ \mathrm{pc}^{-2}$, the exponential scale is $\lambda_d^{-1} = 2.46$ kpc, and $R = |\boldsymbol{\rho}|$ is the galactocentric radius. The luminosity radius is taken as $R_L = 10.8$ kpc (Wevers 1984).

As far as the mass distribution is concerned, the reader is referred to the detailed description by Kent (1987). We take the "full solution case" for the two-component model: thin disk plus spheroidal halo (the galaxy bulge is not relevant here, so we assume $M_b = 0$). The disk surface mass distribution is assumed similar to the light profile

$$\sigma(R) = \sigma_0 e^{-\lambda_d R} , \tag{A2}$$

where $\sigma_0 = 244.7\ M_\odot\ \mathrm{pc}^{-2}$, and the exponential scale is the same as before $\lambda_d^{-1} = 2.46$ kpc. The total extension of the disk mass distribution is taken up to $R_M = 33$ kpc, and the resulting total disk mass is $9.3 \times 10^9\ M_\odot$.

The mass of the halo is given by

$$M(r) = 4\pi\rho_0 a_h^2[r - a_h \arctan (r/a_h)] \tag{A3}$$

where $\rho_0 = 1.63 \times 10^{-23}$ g cm^{-3} is the central dark halo density, and $a_h = 1.3$ kpc is the isothermal halo mass scale length. The resulting total halo mass is $1.5 \times 10^{11}\ M_\odot$.

2. THE MILKY WAY

The expressions for the luminosity and mass distributions are equal to those defined for NGC 3198 (the bulge is assumed as a point source at the center of the disk). The input values in this case are $I_0 = 108.28\ L_\odot\ \mathrm{pc}^{-2}$, the exponential scale is $\lambda_d^{-1} = 5.00 \pm 1.0$ kpc, and the luminosity radius is $R_L = 22.0$ kpc (van der Kruit 1987). The total bulge luminosity is $1.5 \times 10^9\ L_\odot$, which is simply added to the disk center. The bulge radius is about 2.7 kpc, and our "point source" assumption overestimates the radiation force inside this radius. Given the large distances traveled by grains which begin their evolution within this radius, the error introduced by the approximation is not very important.

The mass distribution has been modeled by van der Kruit (1987) with the "maximum disk solution" and taking into account the relevant presence of the bulge. The spherical bulge contributes with a mass of $10^{10}\ M_\odot$, and the disk mass distribution has $\sigma_0 = 381.9\ M_\odot\ \mathrm{pc}^{-2}$ with the same exponential scale as the luminosity profile. The extent of the mass distribution is $R_M = 40$ kpc, and the total mass of the disk is $6 \times 10^{10}\ M_\odot$. The mass of the dark halo is given by a central density $\rho_0 = 6.28 \times 10^{-24}$ g cm^{-3}, and a halo mass scale length of $a_h = 2.8$ kpc, with a total halo mass of $3.0 \times 10^{11}\ M_\odot$.

REFERENCES

Allen, C., & Martos, M. A. 1986, Rev. Mex. Astr. Af., 13, 137
Bahcall, J. N., Schmidt, M., & Soneira, R. M. 1983, ApJ, 265, 730
Barlow, M. J. 1978, MNRAS, 183, 367
Barsella, B., Ferrini, F., Greenberg, J. M., & Aiello, S. 1989, A&A, 209, 349
Bazell, D., & Dwek, E. 1990, ApJ, 360, 142
Beck, R. 1990, in Modern Synthesis Observations of Spiral Galaxies, ed. N. Duric & P. C. Crane, in press
Bouchet, P., Lequeux, J., Maurice, E., Prévot, L., & Prévot-Burnichon, M. L. 1985, A&A, 149, 330
Burstein, D., & Rubin, V. C. 1985, ApJ, 297, 423
Burton, W. B. 1990, in Chemical and Dynamical Evolution of Galaxies, ed. F. Ferrini, J. Franco, & F. Matteucci (Pisa: ETS), 657
Chiao, R. Y., & Wickramasinghe, N. C. 1972, MNRAS, 159, 361
Cox, D. P. 1990, in IAU Symposium 144, The Interstellar Disk-Halo Connection in Galaxies, ed. H. Bloemen, (Dordrecht: Kluwer), 143
Dahlem, M., Koribalski, B., Mebold, U., & Wielebinski, R. 1990, in IAU Symposium 144, The Interstellar Disk-Halo Connection in Galaxies, Poster Proceedings, ed. H. Bloemen, poster book, 39
Danly, L. 1990, in IAU Symposium 144, The Interstellar Disk-Halo Connection in Galaxies, ed. H. Bloemen (Dordrecht: Kluwer), 53

© American Astronomical Society • Provided by the NASA Astrophysics Data System

1991ApJ...381..137F

Désert, F. X., Baxell, D., & Boulanger, F. 1988, ApJ, 334, 815
Devereux, N. A., & Young, J. S. 1990, ApJ, 359, 42
Dickey, J. M., & Lockman, F. J. 1990, ARA&A, 28, 215
Draine, B. T., & Lee, H. M. 1984, ApJ, 285, 89
Draine, B. T., & Salpeter, E. E. 1979, ApJ, 231, 77
Eales, S. A., Wynn-Williams, C. G., & Duncan, W. D. 1989, ApJ, 339, 859
Edgar, R. J., & Savage, B. D. 1989, ApJ, 340, 762
Ferrara, A., Ferrini, F., Barsella, B., & Aiello, S. 1990, A&A, 240, 259
Ferrara, A., Franco, J., Ferrini, F., & Barsella, B. 1989, in IAU Colloquium 120, Structure and Dynamics of the Interstellar Medium, ed. G. Tenorio-Tagle, M. Moles, & J. Melnick (Berlin: Springer), 454
Franco, J., & Cox, D. P. 1986, PASP, 98, 1076
Franco, J., Ferrini, F., Ferrara, A., & Barsella, B. 1991, ApJ, 336, 443
Greenberg, J. M., & Chlewicki, G. 1983, ApJ, 272, 563
Greenberg, J. M., Ferrini, F., Barsella, B., & Aiello, S. 1987, Nature, 327, 214
Hartquist, T. W., & Morfill, G. E. 1986, ApJ, 311, 518
Heiles, C. 1990, in IAU Symposium 144, The Interstellar Disk-Halo Connection in Galaxies, ed. H. Bloemen (Dordrecht: Kluwer), 443
Hoffmeister, C. 1962, Zs. Ap., 55, 46
Hummel, E., Beck, R., & Dahlem, M. 1991, A&A, in press
Hummel, E., van Gorkom, J. H., & Kotanyi, C. G. 1983, ApJ 267, L5
Kent, S. M. 1987, AJ, 93, 816
Kwok, S. 1975, ApJ, 198, 583
Lesch, H., Crusius, A., Schlickeiser, R., & Wielebinski, R. 1989, A&A, 217, 99
Marshall, F. J., & Clarke, G. W. 1984, ApJ, 287, 633
Mathis, J. S. 1973, ApJ, 183, 41
———. 1990, ARA&A, 28, 37
Mathis, J. S., Rumpl, W., & Nordsieck, K. H. 1977, ApJ, 217, 425
Matsumoto, P., & Shibata, K. 1990, in IAU Symposium 144, The Interstellar Disk-Halo Connection in Galaxies, ed. H. Bloemen (Dordrecht: Kluwer), 429
McCammon, D., & Sanders, W. T. 1990, ARA&A, 28, 657
Okroy, R. 1965, Astr. Tsirk., 320, 4
Ostriker, J., Vogeley, M., & York, D. 1990, ApJ, 364, 405
Parker, E. 1966, ApJ, 145, 811
Pence, W. 1976, ApJ, 203, 39
Phillip, H. L. 1977, Phys. Rev., B16, 2896
Puget, J. L., & Léger, A. 1989, ARA&A, 27, 161
Rand, R. J., & Kulkarni, S. R. 1989, ApJ, 343, 760
Reich, W. 1988, in The Galactic Center, ed. M. Morris (Dordrecht: Kluwer), 69
Reynolds, R. J. 1989, ApJ, 339, L29
Rudnicki, K., Wszolek, B., Masi, S., De Bernardis, P., & Salvi, A. 1989, Comm. Ap., 13, 171
Ruzmaikin, A. 1987, in Interstellar Magnetic Fields, ed. R. Beck & R. Gräve (Berlin: Springer), 16
Salpeter, E. E. 1974, ApJ, 193, 585
Savage, B. D. 1989, in Evolution of the Interstellar Medium, ed. L. Blitz (ASP Conf. Ser., 12), 5
Scalo, J. 1990, in Physical Processes in Fragmentation and Star Formation, ed. R. Capuzzo Dolcetta, C. Chiosi, & A. Di Fazio (Dordrecht: Kluwer), 151
Seiradakis, J. H., Lasenby, A. N., Yusef-Zadeh, F., Wielebinski, R., & Klein, U. 1985, Nature, 317, 697
Shull, J. M. 1977, ApJ, 215, 805
Sofue, Y. 1987, PASJ, 39, 547
———. 1990, in IAU Symposium 144, The Interstellar Disk-Halo Connection in Galaxies, ed. H. Bloemen (Dordrecht: Kluwer), 169, 309
Sofue, Y., Fujimoto, M., & Wielebinski, R. 1986, ARA&A, 24, 459
Teerikorpi, P. 1990, A&A, 235, 362
Telesco, C. M., Decher, R., & Joy, M. 1989, ApJ, 343, L13
Tosatti, E., & Bassani, F. 1970, Nuovo Cimento, 65B, 161
Vallée, J. P. 1990, ApJ, 360, 1
van der Kruit, P. C. 1987, in The Galaxy, ed. G. Gilmore & B. Carswell (Dordrecht: Reidel), 27
Véron-Cetty, M. P., & Véron, P. 1985, A&A, 145, 425
Wevers, B. M. H. R. 1984, Ph.D. thesis, Groningen
Williams, D. A. 1989, in IAU Symposium 135, Interstellar Dust, ed. L. J. Allamandola & A. G. G. M. Tielens (Dordrecht: Kluwer), 367
Yoshii, Y., & Takahara, F. 1988, ApJ, 326, 1

© American Astronomical Society • Provided by the NASA Astrophysics Data System